JOURNAL OF SOLID STATE CHEMISTRY **140,** 201–218 (1998)
ARTICLE NO. SC987866

Diffraction and DAFS Studies of a $Ba_4(Ba_xPt^{2+}_{1-x})Pt^{4+}_2O_9$ Twinned Crystal, a Member of the $Ba_p(Ba_xPt^{2+}_{1-x})Pt^{4+}_{p-2}O_{3p-3}$ Series

J. Vacínová[1] and J. L. Hodeau[2]

Laboratoire de Cristallographie CNRS, BP 166X, 38042 Grenoble Cedex, France

Received December 18, 1997; in revised form April 4, 1998; accepted April 10, 1998

Crystallographic studies of the Ba–Pt–O system have been undertaken using X-ray and electron diffraction techniques. The system is described by means of a $Ba_p(Ba_xPt^{2+}_{1-x})Pt^{4+}_{p-2}O_{3p-3}$ formula which corresponds to a BaO_3 hexagonal based framework with Pt chains, where p represents the oxygen deficiency and the presence of both Pt^{4+} and Pt^{2+} cations in the compounds, and x a possible substitution of Pt^{2+} by Ba^{2+} in trigonal prismatic sites. The structure of a $Ba_4(Ba_{0.04}Pt^{2+}_{0.96})Pt^{4+}_2O_9$ crystal has been solved by using 5548 X-ray difraction reflections collected on a twinned crystal. Refinements were performed with two distinct models: an "average" $P321$ space group and an "orthorhombic" $C2$ space group with cell parameters $a = 17.460(4)$ Å, $b = 10.085(2)$ Å, $c = 8.614(3)$ Å. In this structure, two Pt^{4+} and one Pt^{2+} cations are distributed over four Ba planes and form chains along the c axis, consisting of two face-sharing $Pt^{4+}O_6$ octahedra connected with one $Pt^{2+}O_6$ trigonal prism. A lattice misfit occurs between the rigid barium lattice and the PtO_3 chains, giving rise to a composite structure. Twinning and domain configurations are described and taken into account in the refinement. This twinning is related to the presence of Pt^{2+} cations, whose positions break the threefold axis symmetry. A diffraction anomalous fine structure (DAFS) study was also performed on this twinned single crystal. Anomalous scattering factors f' and f'' for platinum in this crystal were refined near the L_{III}Pt absorption edge. They confirm the weak barium occupancy of the trigonal prismataic site and the Pt^{4+} valence of the octahedral sites. Reflection overlaps, due to twinning, flatten the DAFS sensitivity to Pt atoms in the prismatic sites and did not allow their clear valence determination, but Pt–O bond lengths agree with the presence of Pt^{2+} cations at the center of prismatic faces. Electron diffraction patterns of powders having slightly different composition show a continuous evolution of incommensurate Bragg peaks and a weak correlation between the PtO_3 chains. They also confirm the composite nature and the one-dimensionality of the $Ba_p(Ba_xPt^{2+}_{1-x})Pt^{4+}_{p-2}O_{3p-3}$ series, which can produce highly anisotropic physical properties. © 1998 Academic Press

1. INTRODUCTION

In general platinum oxides can be divided into two groups: those containing divalent platinum (Pt^{2+}) with a square planar coordination PtO_4 and those with fully oxidized tetravalent platinum (Pt^{4+}) with an octahedral coordination PtO_6. Numerous examples of these two groups together with their properties have been reported by Schwartz and Prewitt (1).

Our studies were focused on compounds of the Ba/Pt/O system which, depending on Ba/Pt ratio and oxygen content, can contain the platinum cations in both valence states. The phase diagram of this system was first studied by Schneider and McDaniel (2). The structures of several stoichiometric compounds were characterized by Haradem *et al.* (3) ("$Ba_3Pt_2O_7$"), Chamberland (4) and Gallagher *et al.* (5) ($BaPtO_3$), and Wilkinson and Cheetham (6) (Ba_4PtO_6). Most of these compounds have an hexagonal symmetry. However, structures of closely related samples M_4PtO_6(M = Sr (7, 8), M = Sr, Cu (9, 10), M = Ca (11, 12)) have a lower symmetry, related to a particular environment and symmetry of the M cation in the trigonal prismatic site of Pt–M chains (10). Several authors (2–5) have observed a variation of unit cell parameters for the same stoichiometric compounds when they are prepared by different methods. In fact, the stoichiometries for these compounds exhibit different Ba/O, Pt/O, and Ba/Pt ratios, which appear to be connected with oxygen deficiency, as suggested by Gallagher *et al.* (3) in an article describing the existence of $BaPtO_{3-x}$ compounds. Another way of representation of this Ba/Pt/O system is related to the composite structure of $[Ba]_x[(Pt, Cu)O_3]$ reported by Ukei *et al.* (13), it gives a continuous evolution of platinum coordination.

The structural models, determined for the compounds Ba_4PtO_6 (6) and "$Ba_3Pt_2O_7$" (3), are based on a compact stacking of BaO_3 layers of hexagonal –A–B–A–B– type, and they contain chains of different sequences of Pt polyhedra (octahedron or trigonal prism) along the c axis. The refinement of "$Ba_3Pt_2O_7$" shows partially occupied sites and large thermal factors, indicating an average structure. The

[1]Present address: Faculty of Mathematics and Physics UK, Department of Semiconductors, Charles University, Ke Karlovu 5, 121 16 Prague 2, Czech Republic.

[2]To whom correspondence should be addressed. E-mail: hodeau@polycnrs-gre.fr.

0022-4596/98 $25.00

structure of another platinum oxide, Sr_3PtCuO_6 (10) containing (Pt, Cu) chains, reveals that the octahedral and prismatic sites may be occupied by Pt^{4+} and (Pt^{2+}, Cu^{2+}) cations respectively, Cation–oxygen distances (2.00 Å for Pt–O and Cu–O) for these sites are comparable with the Pt^{4+}–O distances in an octahedron and Pt^{2+}–O ones in a square planar coordination.

Ba/Pt/O compounds are one-dimensional materials exhibiting anisotropic physical properties. The closely related compound $Sr_3Cu(Pt_{0.5}Ir_{0.5})O_6$ seems to be an example of a random quantum spin $\frac{1}{2}$ paramagnetic chain (14). Their structure is often partly disordered, and a better understanding of their structure and composition is needed. Our description is based on electron diffraction studies and on the X-ray structural determination of the so-called "$Ba_3Pt_2O_7$" phase which corresponds really to a $Ba_4Pt_3O_9$ stoichiometry. We also compare our results with the representations given by Ukei *et al.* (13) and Grasset *et al.* (16).

To show that the oxygen deficiency and the presence of metallic platinum impurities in $BaPt_{1-y}O_{3-x}$ preparations are related to a structural deformation involving a Pt^{2+}/Pt^{4+} order, we also investigated this system by diffraction anomalous fine structure (DAFS) analysis (15). We report herein the structural relationship between this valence ordering and the platinum coordination.

2. ELECTRON AND X-RAY POWDER DIFFRACTION STUDIES OF THE Ba/Pt/O SYSTEM

2.1. Powdered Ba/Pt/O Compounds from Precursor Preparation

We investigated several compounds prepared by two different ways: by thermal decomposition of a precursor $BaPt(OH)_6$ or by reaction of $BaCO_3$ and PtO_2 (3). The powders prepared from the precursor $BaPt(OH)_6$ were characterized by electron diffraction, and the unit cells of all compounds were determined from X-ray powder patterns. Electron diffraction studies of three different compounds, heated in an oxygen atmosphere at 900, 1000, and 1015°C, show the same crystallographic planes as in the case of a $Ba_4Pt_3O_9$ single crystal (see Part 2.2). They are described with an orthorhombic unit cell, and the parameters were refined as $a_{orth} = 17.4331(14)$ Å, $b_{orth} = 10.0650(8)$ Å, and $c_{orth} = 8.7186(8)$ Å for the 1000°C sample. The powder sample heated at 1015°C shows, beside the reflections corresponding to $Ba_4Pt_3O_9$, extra reflections indicating a loss of metallic platinum.

2.2. Electron Diffraction Study of $Ba_4Pt_3O_9$ Crystals

The pure product was prepared by reaction of $BaCO_3$ and PtO_2, and crystals were grown from a $BaCl_2$ flux in a platinum crucible (3). These crystals, initially called "$Ba_3Pt_2O_7$", were investigated by electron diffraction using a Philips EM400 (120 kV) transmission electron microscope equipped with a goniometric holder allowing crystal orientation along two rotation axes.

Diffraction patterns show a collection of intense spots and weaker reflections. According to the current model, the first ones correspond to the barium lattice with an hexagonal unit cell (basic structure), and the second ones to the platinum and oxygen lattice (superstructure). These and the X-ray precession patterns can be indexed in an orthorhombic unit cell: $a_{orth} = 17.460(4)$ Å, $b_{orth} = 10.085(4)$ Å, and c_{orth} ranging from 8.614(3) to 8.554(4) Å. The modulus of unit cell parameters of the basic structure and of the superstrucrture are related as $a_{base} = \frac{1}{3}a_{orth}$, $b_{base} = \sqrt{3}/3b_{orth}$, and $c_{base} = \frac{1}{2}c_{orth}$. All subsequent diffraction patterns will be indexed using this orthorhombic cell.

The diffraction pattern of the [010] zone shows superstructure reflections $(\bar{2}01)$ and (201) corresponding to a nearly commensurable modulation. Intensities of these two sets of satellite reflections vary from one sample to the other, which indicates crystal twinning (Figs. 1a, b and 2a, b). The diffraction patterns of [010] zones of different crystals from the same batch also show that the ratio between c_{base} and c_{orth} varies and corresponds to other closely related Ba/Pt/O phases. The diffraction patterns of Fig. 1a, b correspond to a $2c_{base}$ superstructure (modulation wave vector along the c axis, $\mathbf{q}_c^* = \frac{1}{2}$), the diffraction pattern Fig. 3 shows an incommensurate superstructure close to $\frac{5}{2}c_{base}$ ($\mathbf{q}_c^* \sim \frac{2}{5}$), which is not perfectly ordered and corresponds to a different sequence of platinum polyhedra along the c axis.

3. STRUCTURAL IMPLICATIONS AND GENERAL STRUCTURAL FORMULA $Ba_p(Ba_xPt^{2+}_{1-x})Pt^{4+}_{p-2}O_{3p-3}$ ($p = 3, 4, 5, \ldots, \infty$)

3.1. Schematic Representation

Electron diffraction analysis of different compounds of the Ba/Pt/O system reveals that all compounds have the same hexagonal basic structure ($a_{base} = 5.82$ Å, $c_{base} = 4.31$ Å), which gives rise to the strong reflections observed in the diffraction patterns. This basic structure is generated by a compact hexagonal packing of BaO_3 planes (–A–B–A–B– packing). Six oxygen atoms, from two consecutive planes A and B, form octahedral cavities which are occupied by Pt^{4+} cations. The oxygen deficiency in some layers gives rise to the existence of trigonal prismatic sites in the structure (Fig. 4). These sites are formed by six oxygen atoms from two planes of the same kind (either A, A or B, B) and can be occupied by either Pt^{2+} or Ba^{2+} cations. Both cations are localized at the level of the deficient plane (Fig. 5). For each $Pt^{4+}/(Pt^{2+}, Ba^{2+})$ ratio, a given polyhedral sequence of octahedra O and prisms P occurs along the c axis.

As shown in Fig. 5 the cell parameter c and the sample stoichiometry are related to the –O–P–stacking in the

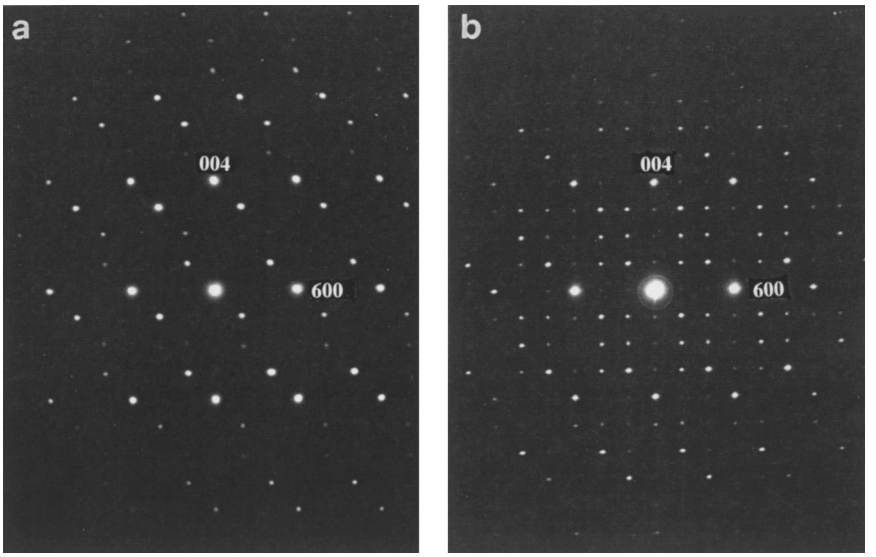

FIG. 1. Electron diffraction patterns corresponding to the [010] zone of two commensurate compounds from the Ba/Pt/O system ($q_c^* = \frac{1}{2}$). (a) A crystal containing one or three crystallographic twins (0, 120, and 240°; see Section 4.3). (b) A crystal containing two or six crystallographic twins.

chains. This variation can be described by the general formula:

$$Ba_p(Ba_xPt^{2+}_{1-x})Pt^{4+}_{p-2}O_{3p-3},$$

where the parameter p corresponds to the number of barium planes and x describes the mixed occupancy of these prismatic sites by Pt^{2+} and Ba^{2+} cations. This formula is close to that proposed by Ukei *et al.*: $Ba_x(Pt, Cu)O_3$ (13). However, it allows us to distinguish the occupations of Pt^{4+} and (Pt^{2+}, Ba^{2+}) and relates them to the oxygen deficiency. The $Ba_p(Ba_xPt^{2+}_{1-x})Pt^{4+}_{p-2}O_{3p-3}$ series can exist for $p = 3, 4, 5, \ldots, \infty$ (see known members of this series in Table 1).

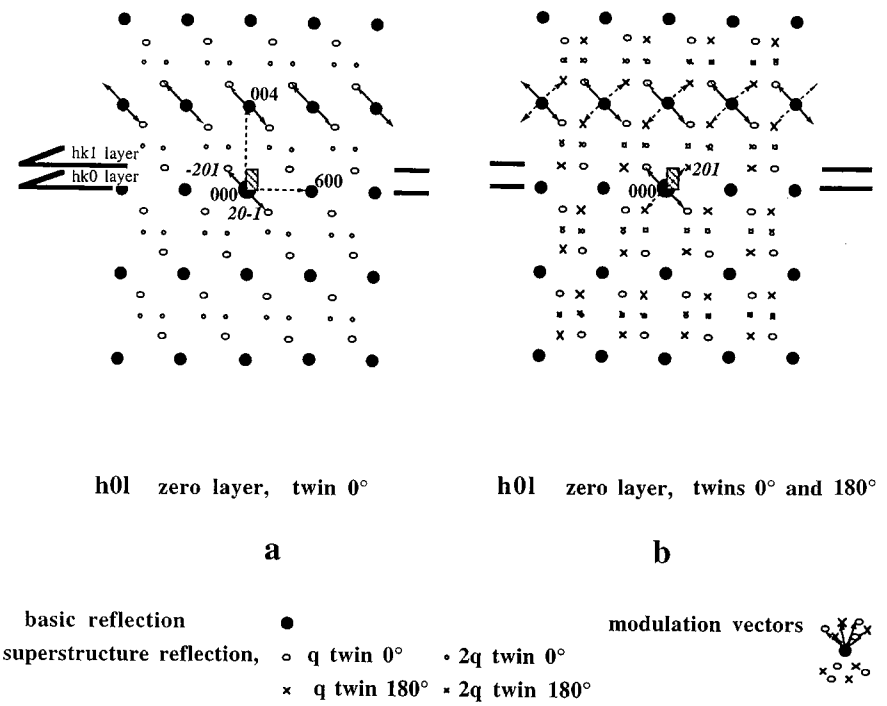

FIG. 2. Schematic representation of diffraction patterns of the [010] zone, showing the modulation satellites ($q_c^* = \frac{1}{2}$). (a) A crystal containing one crystallographic twin. (b) A crystal containing two crystallographic twins.

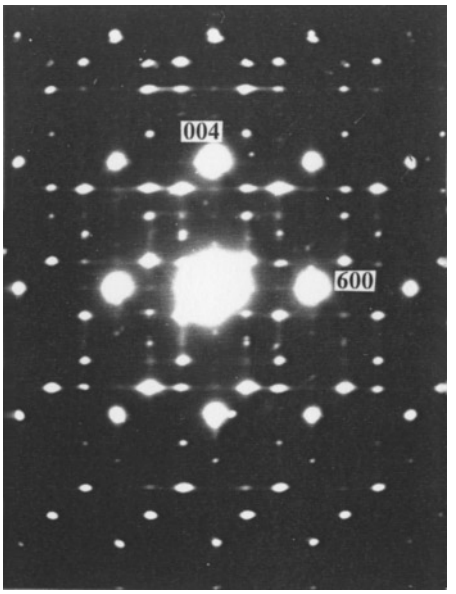

FIG. 3. Electron diffraction patterns of the [010] zone of an incommensurate compound from the Ba/Pt/O system ($q_c^* \sim \frac{2}{5}$).

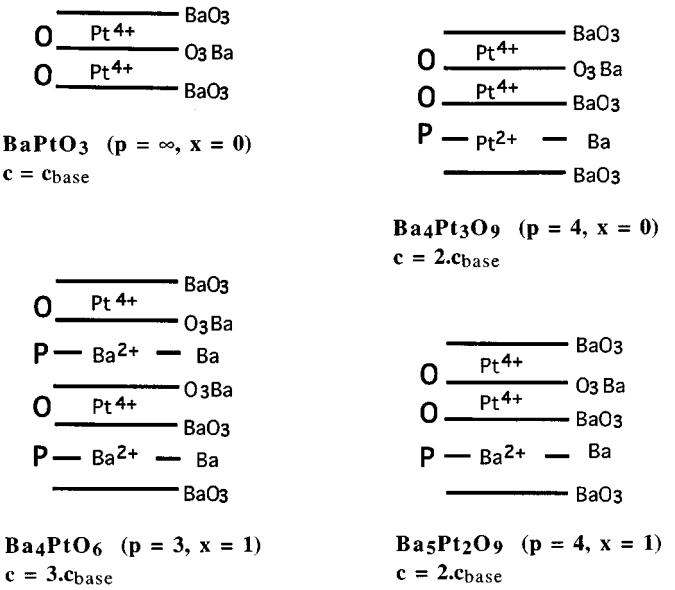

FIG. 5. Different crystallographic phases of the Ba/Pt/O system containing the different sequences of $Pt^{4+}O_6$, $Pt^{2+}O_6$, or BaO_6 polyhedra.

Another representation developed for ruthenium oxides (17) was also proposed for these Ba/Pt/O series (16). All three representations are equivalent and point out the composite nature of these phases.

3.2. Modulation Along the c Axis

For some compounds of this system, a misfit between the Ba and the Pt stacking occurs and the periodicity of polyhedral chains can be incommensurate with the periodicity of the Ba planes (Fig. 6). The modulation wave vector along the c axis $\mathbf{q}_c^*$ corresponds to the ratio of the number of prismatic planes to the number of basic unit cells, hence it is directly connected with the p parameter: $\mathbf{q}_c^* = 2/p$. It varies continuously and could reach commensurable values 0, $\frac{1}{2}$, and $\frac{2}{3}$. For $x = 0$, these values correspond to the stoichiometric compounds $BaPtO_3$, $Ba_4Pt_3O_9$, and $Ba_3Pt_2O_6$, which can be described with a supercell along the c axis. However, as reported by Ukei *et al.* (13), in the majority of cases it is more convenient to describe this system with an incommensurable structure which represents the mutual periodicity of barium planes and polyhedral chains where anions are strongly bonded to Pt or Cu cations.

The barium cations act as a screen between the platinum chains and we can observe no correlation of the order of prismatic sites in one chain with respect to those in neighboring chains. This possible interchain disorder explains the diffuse pattern (Fig. 3), which can occur in planes perpendicular to the c axis, at a $\mathbf{q}_c^*$ parameter corresponding to a given –P–O– sequence in the compound.

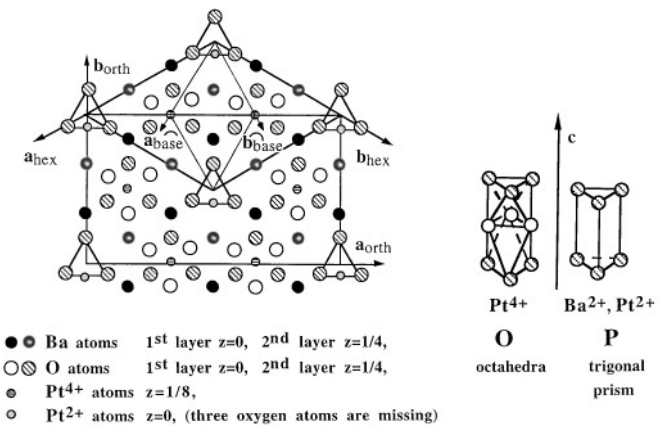

FIG. 4. Hexagonal packing of two consecutive BaO_3 planes (–A–B–) along the c axis, position of platinum chains, and schematic representation of polyhedral cavities in the structure. The octahedral sites O are between two complete BaO_3 planes, the prisms P are among three planes where the middle one is deficient in oxygen.

3.3. Symmetry of Compounds of Ba/Pt/O Series

In $BaPtO_3$, the platinum chains are formed only by PtO_6 octahedra. The Pt–O distances ~ 2 Å correspond to a typical local environment of Pt^{4+} cations in between two BaO_3 planes (1). The c axis of this compound is equal to $c = c_{base}$. The structure of Ba_4PtO_6 (6) is compatible with the model illustrated in Fig. 5 where one of three barium planes is deficient in oxygen. The chains are formed by a sequence of octahedra and prisms –O–P–O–P– which are occupied by

TABLE 1
Platinate Compounds Described by the $Ba_p(Ba_xPt^{2+}_{1-x})Pt^{4+}_{p-2}O_{3p-3}$ Formula

$Ba_p(Ba_x,Pt^{2+}_{1-x})Pt^{4+}_{p-2}O_{3p-3}$	Chain stacking	p	x	q_c^*	q_c (supercell)	References
$Ba\,Pt^{4+}O_3$	–O–O–O–O–O–O–	∞		0	c	5
$Ba_6(Ba, Pt^{2+})_1Pt^{4+}{}_4O_{15}$	–O–O–O–O–P–	6	x	1/3	3c	
$Ba_5(Ba, Pt^{2+})_1Pt^{4+}{}_3O_{12}$	–O–O–O–P–	5	x	2/5	2.5c; 5c	Herein Fig. 3
$Ba_4(Ba, Pt^{2+})_1Pt^{4+}{}_2O_9$	–O–O–P–	4	x	1/2	2c	Herein
$Ba_4Pt^{2+}{}_1Pt^{4+}{}_2O_9$	–O–O–P–	4	.04	1/2	2c	Herein
"$Ba_3Pt_2O_7$"	–O–O–P–	4	$\sim$ .2	1/2	2c	3
"Ba_2PtO_4"	–O–O–P–	4	$\sim$ .66	1/2	2c	2
$Ba_5Pt^{4+}{}_2O_9$	–O–O–P–	4	1.0	1/2	2c	16
$Ba_3(Ba, Pt^{2+})_1Pt^{4+}{}_1O_6$	–O–P–	3	x	2/3	1.5c; 3c	
$Ba_4Pt^{4+}O_6$	–O–P–	3	1.0	2/3	1.5c; 3c	2, 6
$Sr_4Pt^{4+}O_6$	–O–P–	3	1.0 (Sr)	2/3	1.5c; 3c	7, 8
$Ca_4Pt^{4+}O_6$	–O–P–	3	1.0 (Ca)	2/3	1.5c; 3c	11, 12
Ba_3 (Cu, $Pt^{2+})_1Pt^{4+}O_6$	–O–P–	3	x (Cu)	2/3	1.5c; 3c	13
$Sr_3Cu^{2+}Pr^{4+}O_6$	–O–P–	3	.0 (Cu)	2/3	1.5c; 3c	9, 10

Pt^{4+} and Ba^{2+} cations, respectively ($p = 3$, $x = 1$). One unit cell contains the sequence –O–P–O–P– distributed over six barium planes, the hexagonal c axis is $c_{hex} = 3c_{base}$. This structure is comparable to that of Sr_3PtCuO_6 (9, 10), where Sr cations replace Ba ones in the basic framework, and the crystallographic sites in the chains –O–P–O–P– are occupied by Pt^{4+} cations (octahedra) and Cu^{2+} cations (trigonal prisms). Contrary to $BaPtO_3$ and Ba_4PtO_6 which conserve hexagonal or rhombohedral symmetry, Sr_3PtCuO_6 is monoclinic. This lower symmetry is directly connected to the occupancy of the prismatic sites, where the Cu^{2+} cations are situated in the center of one of the three rectangular faces,

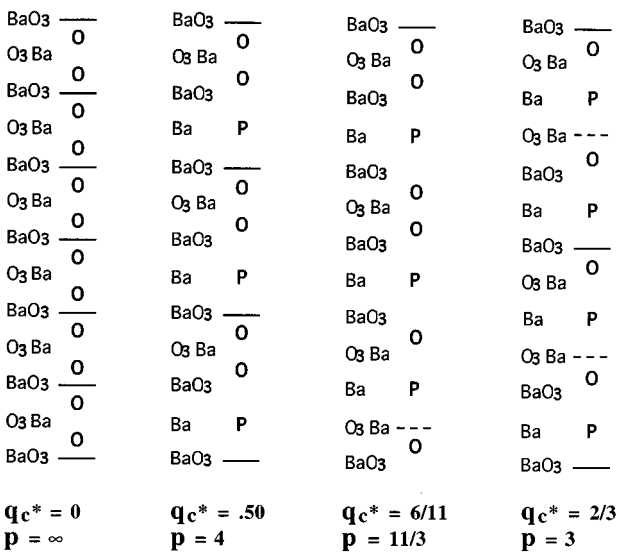

FIG. 6. Modulation along the c axis for different sequences of O and P sites in the polyhedral chains.

with a square planar coordination CuO_4. Owing to the Cu^{2+} localization, the threefold axis disappears and the compound forms twins generated by a pseudothreefold axis. This phenomena also exists in Ba/Pt/O series because the Pt^{2+} cations show a strong preference for a square planar coordination with Pt–O distances close to 2 Å (1). The 3-fold axis suppression and the corresponding twinning can be interpreted as an indicator of the presence of Pt^{2+} cations in the compound, localized on one of the three rectangular faces of trigonal prisms.

4. STRUCTURAL DETERMINATION OF $Ba_p(Ba_xPt^{2+}_{1-x})Pt^{4+}_{p-2}O_{3p-3}$ ($p = 4$, $x \ll 1$) CRYSTALS

4.1. Analysis of Previous Structural Model Proposed for These Crystals

The structure of a "$Ba_3Pt_2O_7$" compound with a stoichiometry close to $Ba_4Pt_3O_9$ was described by Haradem *et al.* (3) using a hexagonal unit cell and the space group $P\bar{6}2c$. In this model there exist three different platinum chains. The first one corresponds to the stacking of four face-shared octahedra (–O–O–O–O–), but the short Pt–Pt distances indicate that these octahedra cannot be fully occupied at the same time. The second and third platinum chains are formed by an –O–O–P– stacking of only three sites, shifted with respect to one another. Comparing this structural model to the general model proposed above one can conclude that the –O–O–O–O– chains are probably an artifact imposed by the symmetry of the space group $P\bar{6}2c$.

In the –O–O–P– chains, this previous structural analysis also shows a disorder of platinum atoms, which tend to move forward to centers of the rectangular faces in the trigonal prisms. This disorder can be imposed by too high symmetry and could indicate the presence of Pt^{2+} cations

on one of the three rectangular faces inducing the lower symmetry for the compound.

To test our model and to solve these structural imcompatibilities, we studied several single crystals of this phase using the precession method, and we refined their structure using the set of 9234 intensities collected on a twinned crystal.

4.2. Modulation and Twinning in the $Ba_4Pt_3O_9$ Crystals

Precession patterns of different (0k0) planes show that this compound exhibit a weak incommensurability (Fig. 7a).

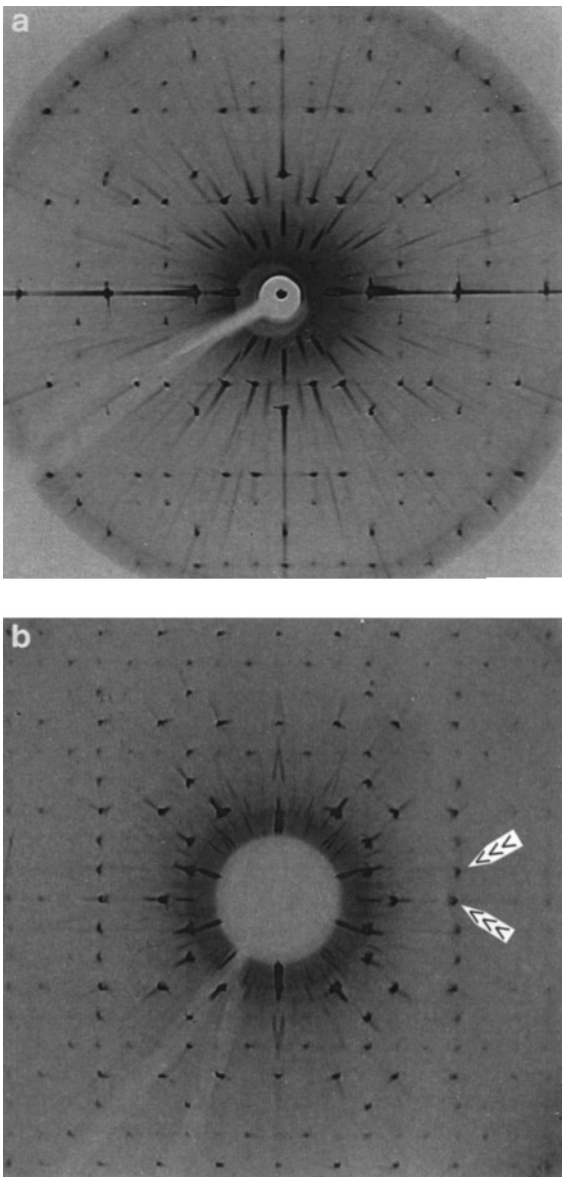

FIG. 7. Diffraction pattern of the $h0l$ (a) and $h2l$ (b) layer of a $Ba_4Pt_3O_9$ crystal obtained by the precession method. The arrow of the (b) pattern quotes the incommensurability of this crystal ($q_c^* = 0.507$).

This can be easily seen on the layer $h2l$ where we measure a modulation wavevector $\mathbf{q}_c^* = 0.507(2)$ (Fig. 7b). For different crystals from the same batch, this incommensurate wavevector varies between 0.5 and 0.514.

The width of reflections with odd indexes l, arising from the superstructure is about two or three times larger than the corresponding one from the basic structure ($l = 2n$ and $h = 3 \times 2n$, $k = 2n$, or $h = 3(2n + 1)$, $k = 2n + 1$). The perpendicular elongation of the superstructure reflections with respect to the c axis indicates a partial ordering decorrelation between platinum chains.

A detailed intensity analysis of the diffraction spots indicates that all crystals are twinned and consist of several domains. The diffraction patterns reveal a pseudohexagonal symmetry and the distribution of reflection intensities indicates a pseudotrigonal symmetry. This is produced by three principal domains of comparable sizes which are related by a threefold axis parallel to the c axis and three smaller domains turned by 60° with respect to previous ones.

As can be seen in Fig. 8, diffraction patterns can be described with an orthorhombic unit cell and twins generated by a rotation around a pseudotrigonal or a pseudohexagonal axis. The corresponding unit cells are $a_{orth} = 17.460(4)$ Å, $b_{orth} = 10.085(2)$ Å, and $c_{orth} = 8.554(3)$ Å for the orthorhombic superstructure cell and $a_{base} = 5.820(2)$ Å and $c_{base} = 4.277(2)$ Å for the hexagonal basic cell (Fig. 8b, c).

4.3. Experimental Conditions and Corrections for the Measured Intensities

The morphology of the sample selected for the four circle diffractometry is well described as a small parallelepiped of dimensions $150 \times 130 \times 70$ μm defined by its crystallographic faces. This sample was mounted on an automatic Nonius diffractometer using Ag$K\alpha$ radiation and equipped with a graphite monochromator.

Owing to a relatively weak deviation from the commensurability, $\mathbf{q}_c^* = 0.5071(3)$, we described the reflection positions with an approximative commensurate hexagonal cell. Its parameters were refined using the positions of 25 reflections collected over the interval $22 \leq 2\theta \leq 40°$. Due to the small discrepancy between measured and calculated positions, the detector slits were opened to 5×4 mm^2. Intensities of Bragg reflections were collected for a complete sphere of reciprocal space, up to $2\theta = 50°$ in the ω scan mode. A large scanning interval ($\Delta\omega = 2.5°$) was chosen because of the large width of reflections (superstructure FWHM $\Delta\omega = 0.5$–$0.8°$, basic structure FWHM $\Delta\omega = 0.3$–$0.4°$) and the weak incommensurability of the compound.

The measured intensities were converted into structure factors after Lorentz, polarisation corrections and

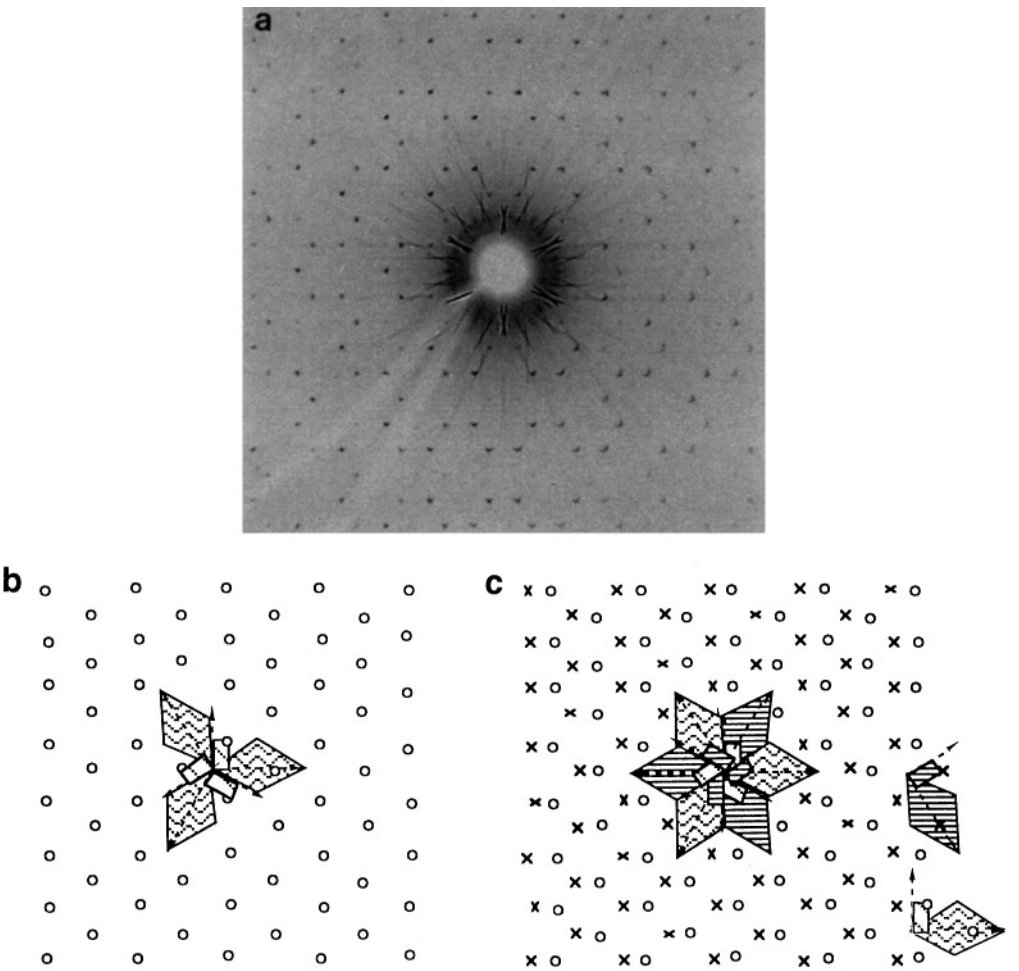

FIG. 8. *hkl* reciprocal layer of a twinned crystal $Ba_4Pt_3O_9$. (a) Diffraction pattern obtained by the precession method. (b) Schematic representation with three twins, P0, P1, P2. (c) Schematic representation with six twins: P0, P12, P1, P10, P2, P11.

absorption correction calculated with a program using the geometric shape of crystal. The linear absorption coefficient of the compound for Ag$K\alpha$ radiation is equal to $\mu = 282.1\ cm^{-1}$, and the transmission coefficient varied from 0.0037 to 0.1442.

From the 9234 measured reflections only 5548 with $F > 5\sigma(F)$ were used in the structural refinements. Structural factors were calculated using the scattering factors of Cromer and Waber (18), and the anomalous factors f' and f'' of Cromer and Liberman (19). Structural refinements were carried out using the MXD least-squares program (20). This program was chosen owing to its capabilities for the refinement of nonstandard structures (modulation, twinning, ...). The refinements were undertaken either on observed structural factors (hexagonal cell) or on intensities (orthorhombic cell + twinning) with a reflection weight $1/\sigma$.

4.4. Refinement Using the Hexagonal Cell and P321 Symmetry

As a starting model we used the structure proposed by Haradem *et al.* (3) with the hexagonal unit cell and the space group $P\bar{6}2c$. The refinement converged to a weighted least-squares factor of $R_w \approx 30\%$.

Furthermore no systematic extinction was observed, so we described the compound in space group $P321$ and the hexagonal unit cell $a_{hex} = 10.085(2)$ Å and $c_{hex} = 8.554(3)$ Å. In this model we assumed that the packing of four –A–B–A–B– layers consists of three BaO_3 layers and one Ba layer deficient in oxygen. This corresponds to a stoichiometric formula $Ba_4Pt_3O_9$ ($p = 4$ and $x = 0$ in the general formula, Fig. 5). The oxygen vacancies create two types of crystallographic sites along the c axis. The octahedral sites are occupied by Pt^{4+} cations, and the trigonal prism is

TABLE 2
Initial and Final Atomic Positions Using the Structural Description with a Space Group *P*321

Atom	Position	x	y	z	x	y	z
Ba(1)	3e	1/3	0	0	0.348(1)	0	0
Ba(2)	3f	1/3	0	2/4	0.340(1)	0	1/2
Ba(3)	6g	2/3	0	1/4	0.6859(8)	0.0258(7)	0.2526(7)
Pt(1)(Pt^{2+})	3e	0	0.91	0	0	0.908(2)	0
Pt(2)	2c	0	0	3/8	0	0	0.3330(8)
Pt(3)(Pt^{2+})	6g	3/4	1/3	6/8	0.718(1)	0.335(1)	0.763(1)
Pt(4)	2d	2/3	1/3	3/8	2/3	1/3	0.4122(6)
Pt(5)	2d	2/3	1/3	1/8	2/3	1/3	0.0971(6)
O(1)	6g	1/6	2/3	0	0.17(2)	0.70(2)	0.00(2)
O(2)	6g	1/6	2/3	2/4	0.08(2)	0.70(2)	0.45(2)
O(3)	3f	5/6	0	2/4	0.86(3)	0	1/2
O(4)	6g	1/6	0	3/4	0.15(1)	0.00(1)	0.800(7)
O(5)	6g	5/6	1/3	1/4	0.84(1)	0.34(1)	0.267(8)

TABLE 3
Initial Positions of Ba and Pt Atoms Using the Structural Description with Space Group *C*2; They Correspond to Ideal –O–O–P– Chains and Ideal Pt^{2+} Positions at the Center of One Rectangular Face of the Trigonal prism

Atom	Position	x	y	z
Ba(1)	2a	0	1/3	0
Ba(2)	4c	1/3	1/3	0
Ba(3)	4c	1/6	1/6	1/4
Ba(4)	4c	1/2	1/6	1/4
Ba(5)	4c	5/6	1/6	1/4
Ba(6)	2b	0	1/3	2/4
Ba(7)	4c	1/3	1/3	2/4
Pt(1) (Pt^{2+})	2a	0	0.95833	0
Pt(2)	4c	0	0	3/8
Pt(3) (Pt^{2+})	4c	1/3	0.04167	6/8
Pt(4)	4c	1/3	0	1/8
Pt(5)	4c	1/3	0	3/8

occupied by a Pt^{2+} cation placed on one of its rectangular faces.

In the *P*321 space group, each prismatic site provides three possibilities of simultaneous occupancy by Pt^{2+} cations, so we introduced in each site a Pt^{2+} population equal to $\frac{1}{3}$. In our model each structural unit along the c axis is formed by two face-sharing octahedra connected with one trigonal prism (–O–O–P– chains). The trigonal prisms, which are on the $(\frac{2}{3}, \frac{1}{3}, z)$ and $(\frac{1}{3}, \frac{2}{3}, z)$ rows of the hexagonal cell, are rotated by 180° with respect to those on the $(0, 0, z)$ row. The refinement using *P*321 non-special positions for all atoms has converged with agreement factors $R_w = 17.5\%$ and $R = 20.7\%$. The final atomic positions are given in Table 2. The cations Pt1 and Pt3 moved away from the threefold axis, which indicates in occupancy of prismatic sites by Pt^{2+} cations rather than by Ba cations ($x \ll 1$).

4.5. Refinement with the Orthorhombic Cell, Twins, and Translation Domains

As intensity distribution and diffusion lines indicate a partial disorder and a twinning of the crystal, we reduced the sample symmetry and described the structure by an orthorhombic unit cell with *C*2 space group, which excludes a simultaneous occupation of Pt^{2+} cations on the three rectangular faces of the trigonal prisms. In view of the studies reported on Sr_3PtCuO_6 crystal (10), the symmetry of the $Ba_4Pt_3O_9$ compound can be monoclinic if twin dimensions are small enough to allow a metrically orthorhombic cell.

Keeping the same structural elements, we converted the hexagonal cell into an orthorhombic one: $a_{orth} = 17.460(4)$ Å, $b_{orth} = 10.085(2)$ Å, and $c_{orth} = 8.554(3)$ Å. The Miller indices were transformed as $h_{orth} = h_{hex} - k_{hex}$, $k_{orth} = h_{hex} + k_{hex}$, $l_{orth} = l_{hex}$. The initial positions of cations are listed in Table 3.

4.5.1. Representation of merihedral twins. The pseudohexagonal symmetry can be interpreted using two different kinds of merihedral twins. The first kind is created by a rotation of 120° around the c axis: $h_{n+1} = -h_n/2 + 3k_n/2$, $k_{n+1} = -h_n/2 - k_n/2$ ($n = 0, 1, 2$); the second by a rotation of 60° around the c axis: $h_{n+1} = -h_n/2 + 3k_n/2$, $k_{n+1} = -h_n/2 + k_n/2$ ($n = 0, 1, 2, 3, 4, 5$, corresponding to individuals quoted P0, P12, P1, P10, P2, P11, respectively; see Fig. 8b, c). These twinned individuals (Fig. 9a) were introduced in the model and the refinement was carried out, using the summation of intensity contributions from each individual Bragg reflection. Only the twin proportions and cations positions were refined, since by a rotation operation the oxygen atoms are practically found on the same positions. The proportions of different twins are given, together with agreement factors, in Table 4. Results of these refinements show that the pseudohexagonal symmetry is produced by six twinned individuals connected by a sixfold axis parallel to the crystallographic c axis. Each individual is associated to an ideal distribution of –O–O–P– chains and Pt^{2+} positions inside trigonal prism P, close to the initial values given in Table 3.

4.5.2. Translation microdomains. The distribution of three platinum atoms on four barium planes along the c axis facilitates the interchain disorder along this axis (Fig. 10a). This absence of correlation induces diffuse streaks perpendicular to the c axis and also an intensity variation of the satellite reflections. In the proposed structural model, this partial disorder was interpreted in a microdomain scale by the presence of stacking faults in the –O–O–P– sequence, giving rise to translated microdomains elongated along the

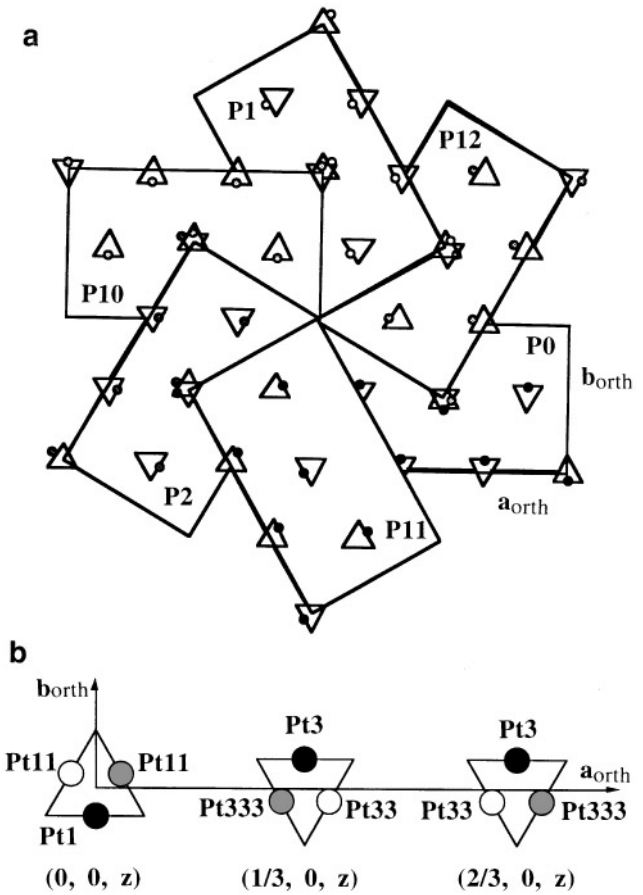

FIG. 9. Twinning and Pt^{2+} local order representation. (a) Large orthorhombic twin individuals: P0, P12, P1, P10, P2, P11 (cf. Section 4.5.1). (b) Pt^{2+} positions on trigonal prism faces (Pt1, Pt11, Pt3, Pt33, and Pt333), deduced by a 120° rotation around the *c* axis (cf. Section 4.5.3).

c axis (the size of microdomains is assumed to be small with respect to coherently diffracting regions). Since by simple translation operations the barium atoms are nearly invariant, we have maintained the rigid barium lattice. The oxygen and platinum atoms were then introduced with positions and occupancies corresponding to translation domains. All possible domains corresponding to the crystal symmetry are schematized in Fig. 10b.

The refinement of fractions of distinct translation domains, twinned individuals, and atomic positions converged with agreement factors $R_w = 12.7\%$ and $R = 10.1\%$. As this model better describes the real structure, the oxygen positions were also refined. At this stage, the refinement gave fractions of the domains D10, D11, and D12 equal to zero, and the values of 0.559(6), 0.222(9), and 0.219(9) for the domains D0, D1, and D2, respectively. The absence of D10–D11–D12 domains is consistent with the fact that they lead to large deformations ("fish bone" type faults), which are energetically unfavorable. In the following refinements only the translation domains D0, D1, and D2 were considered. A schematic representation of the structure containing these three crystallographic domains is given in Fig. 11.

Our results are in agreement with the structural studies on $Ba_x(Pt, Cu)O_3$ reported by Ukei *et al.* (13), who used a continuous model of a composite structure with a rigid barium lattice. We found a deformation of the compact packing produced by oxygen-deficient planes and associated with platinum distribution. This deformation influences the position of the barium atoms which implies that barium atoms must also be introduced into translation domains. The corresponding structural refinement converged with agreement factors $R_w = 12.06\%$ and $R = 9.28\%$. It means that the O–Ba bonds in the Ba/Pt/O system are strong enough, and we cannot simply consider this structure as a purely composite one with two independent lattices, Ba and (PtO_3).

4.5.3. Intraprism Pt^{2+} local order. Due to the possibility of distinct crystallographic sites on the three rectangular faces of each trigonal prism, the Pt^{2+} cations (denoted Pt1 and Pt3 in the orthorhombic structural model reported in Table 3) can also be placed in atomic positions Pt11 (0, $-23/24$, 0), Pt33 (9/24, $-1/24$, $\frac{3}{4}$), or Pt333 (7/24, $-1/24$, $\frac{3}{4}$). The refinements of these new atomic positions, together with the proportions of twins and translation domains, gave the best results for two pairs of Pt^{2+} positions: Pt1 and Pt33 ($R_w = 10.76\%$ and $R = 7.67\%$), Pt1 and Pt333 ($R_w = 10.24\%$ and $R = 7.52\%$). The disorder in the prismatic sites at the atomic scale is represented by the atoms Pt1, Pt11,

TABLE 4
Results of the Refinement with the Merihedral Twins Having a Threefold and/or Sixfold Axis

	Agreement factors		Twin ocupancies					
Type of twins	*R* (%)	R_w (%)	P0 (0°)	P12 (60°)	P1 (120°)	P10 (180°)	P2 (240°)	P11 (300°)
3-fold axis	27.0	32.8	0.31(1)		0.34(1)		0.35(1)	
6-fold axis	19.3	21.1	0.217(8)	0.111(8)	0.241(8)	0.087(7)	0.243(8)	0.102(8)

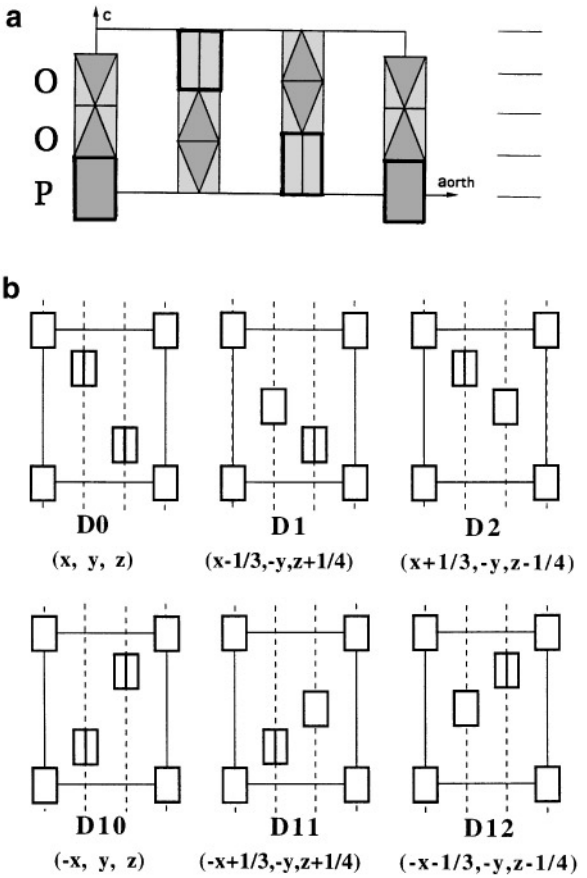

FIG. 10. Schematic projection of the structure on the (a, c) plane. (a) –O–O–P– chains. (b) Translation domains D0, D1, D2, D10, D11, and D12; the prismatic sites are represented by rectangles.

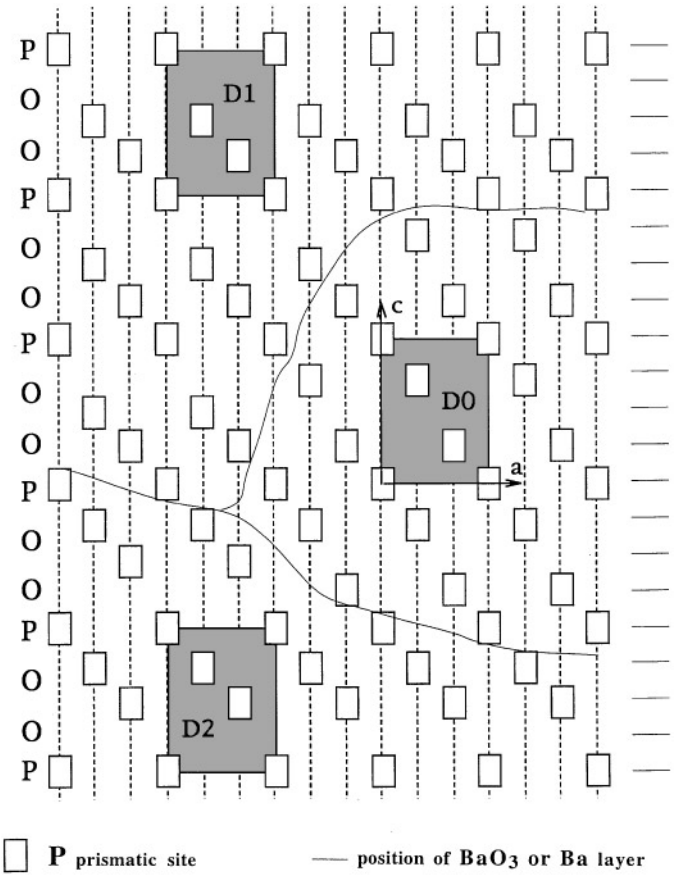

FIG. 11. Schematic projection of the structure and faults in the (a, c) plane with three translation domains: D0; $t = (0, 0, 0)$; D1, $t = (-\frac{1}{3}, 0, \frac{1}{4})$; and D2, $t = (\frac{1}{3}, 0, -\frac{1}{4})$ (gray rectangles are the corresponding unit cells). These three domains correspond to a regular distribution of trigonal prism in planes close to $(\bar{2}01)$ ones, without zigzag (or "fish bone") faults in the trigonal prism distribution.

Pt3, Pt33, and Pt333, the positions of which are schematized in Fig. 9b. Due to the twofold axis along the crystallographic b axis, only two independent cations Pt1 and Pt11 can be introduced into the platinum chains passing through the origin.

The refinement of populations (normalized to sum equal to 1) of Pt1, Pt11, Pt3, Pt33, and Pt333 sites on the prismatic faces converged to $R_w = 7.32\%$ and $R = 5.58\%$ (see Table 5). The most important domain corresponds to a Pt^{2+} occupation of sites Pt1 in the $(00z)$ chain and Pt33 in the $(\frac{1}{3}, 0, z)$ and $(\frac{2}{3}, 0, z)$ chains (given in coordinates of the orthorhombic unit cell).

4.5.4. Mixed occupancy in prismatic sites ($Ba_xPt^{2+}_{1-x}$). The structural model of the Ba/Pt/O system allows the mixed occupation of prismatic sites either by Pt^{2+} or by Ba^{2+} cations. We have attempted to substitute all the Pt^{2+} cations by barium atoms located in the center of the prisms. This model corresponds to the stoichiometric formula $Ba_5Pt_2O_9$ and is schematized in the Fig. 5. Keeping all the structural parameters fixed and refining only the scale factor yielded residuals $R_w = 39\%$ and $R = 30\%$. This clearly shows that Pt^{2+}, and not Ba^{2+} cations, occupy the prismatic sites. In the final refinement, the mixed occupancy factor was $x = 0.043(6)$.

4.6. Structure Description of $Ba_4(Ba_xPt^{2+}_{1-x})Pt^{4+}_2O_9$, with $x = 0.043(6)$

Using the orthorhombic cell, we finally refined all atomic positions, the populations of twins, translation domains, and global thermal factors U. In spite of the risk of correlation effects this refinement converged to $R_w = 6.73\%$ and $R = 5.23\%$. Compared with previous refinements, the oxygen positions varied only slightly. The final atomic parameters and the interatomic distances are summarized in Tables 6 and 7, while the final populations of twinned individuals, translation domains and Pt^{2+} sites are given in Table 5, The structure of the main domain is shown in Fig. 12a, b.

TABLE 5

Population of Twins Generated by a Rotation around a Pseudohexagonal Axis, Population of Translation Domains, and Pt^{2+} Sites

Twins			Domains	Translation vector or rotation angle	Population
P0	0°	0.233(4)	D0	(0, 0, 0)	0.653(7)
P12	60°	0.091(4)	D1	$(-\frac{1}{3}, 0, \frac{1}{4})$	0.169(5)
P1	120°	0.221(4)	D2	$(\frac{1}{3}, 0, -\frac{1}{4})$	0.178(6)
P10	180°	0.112(4)			
P2	240°	0.234(4)	Pt^{2+} sites	Face orientation or rotation angle	Population
P11	300°	0.109(4)			
			Pt1	0°	0.44(1)
			Pt3	0°	0.249(9)
			Pt11	120°	0.26(1)
			Pt33	120°	0.40(1)
			Pt11	240°	0.26(1)
			Pt333	240°	0.31(1)
			Ba(x)	Center of prism	0.043(6)

TABLE 6

Atomic Coordinates, Occupancy, and Isotropic Thermal Factors for the Phase $Ba_4(Ba_xPt^{2+}_{1-x})Pt^{4+}_2O_9$, Corresponding to the Final Refinement ($Rw = 6.73\%$, $R = 5.23\%$); Standard Deviations σ Are Giving in Parentheses

Atom	Site	x	y	z	Population	U (Å^2)
Pt1	2*a*	0	0.9469(16)	0	0.44(1)	0.0038(3)
Pt11	4*c*	0.0291(09)	0.0556(10)	−0.0003(22)	0.26(1)	0.0038(3)
Pt2	4*c*	0.0042(06)	0.0019(15)	0.3361(08)	1	0.0038(3)
Pt3	4*c*	0.3415(13)	−0.0064(41)	0.7827(08)	0.249(9)	0.0038(3)
Pt33	4*c*	0.3698(06)	−0.0308(14)	0.7749(08)	0.40(1)	0.0038(3)
Pt333	4*c*	0.2912(07)	−0.0462(13)	0.7416(11)	0.31(1)	0.0038(3)
Pt4	4*c*	0.3385(04)	0.0021(15)	0.4203(05)	1	0.0038(3)
Pt2	4*c*	0.3366(04)	0.0038(14)	0.1018(05)	1	0.0038(3)
Ba1	2*a*	0	0.3461(18)	0	1	0.0063(4)
Ba2	4*c*	0.3199(9)	0.3194(18)	0.0064(13)	1	0.0063(4)
Ba3	4*c*	0.1637(7)	0.1402(13)	0.2406(11)	1	0.0063(4)
Ba4	4*c*	0.4968(7)	0.1721(14)	0.2645(11)	1	0.0063(4)
Ba5	4*c*	0.8426(9)	0.1826(12)	0.2562(11)	1	0.0063(4)
Ba6	2*b*	0	0.3401(15)	0.5	1	0.0063(4)
Ba7	4*c*	0.3370(6)	0.3231(10)	0.5220(09)	1	0.0063(4)
O1	4*c*	0.239(4)	0.085(08)	−0.014(09)	1	0.0017(29)
O2	4*c*	0.415(5)	0.073(09)	−0.017(09)	1	0.0017(29)
O3	4*c*	0.165(6)	0.349(13)	0.060(11)	1	0.0017(29)
O4	4*c*	0.015(4)	0.138(08)	0.186(08)	1	0.0017(29)
O5	4*c*	0.329(7)	0.157(15)	0.276(11)	1	0.0017(29)
O6	4*c*	0.412(6)	0.428(11)	0.209(08)	1	0.0017(29)
O7	4*c*	0.578(8)	0.418(15)	0.184(12)	1	0.0017(29)
O8	4*c*	0.770(4)	0.400(07)	0.263(08)	1	0.0017(29)
O9	4*c*	0.900(5)	0.429(10)	0.279(10)	1	0.0017(29)
O10	4*c*	0.082(7)	0.074(14)	0.502(15)	1	0.0017(29)
O11	4*c*	0.256(7)	0.079(12)	0.573(11)	1	0.0017(29)
O12	4*c*	0.406(6)	0.092(08)	0.566(11)	1	0.0017(29)
O13	4*c*	0.156(3)	0.380(05)	0.404(06)	1	0.0017(29)
O14	2*b*	0	0.851(18)	0.5	1	0.0017(29)

The refined Pt–O distances are close to a typical local environment of Pt^{2+} and Pt^{4+} cations. For Pt^{4+} cations, they form six Pt–O bonds ranging from 1.79 to 2.17 Å, and all O–Pt–O angles joining the opposite apexes of an octahedron are greater than 158°. The four short Pt^{2+}–O distances in the prisms range from 1.83 to 2.37 Å, and all O–Pt–O angles joining the opposite apexes of the square planar site are greater than 164°, indicating that the Pt^{2+} cation lies practically on one rectangular face of prisms. The Ba coordination varies between 8 and 10 neighbors. One O–O distance was too small (2.29 Å), others are greater than 2.40 Å. The fact that the local environment of platinum cations remains stable and gives reasonable Pt–O distances justificies the structural model proposed for this compound, However, the global thermal factor of oxygen atoms ($U = 0.002(3)$) obtained in this refinement is still too weak.

The crystallographic structure of the $Ba_4(Ba_xPt^{2+}_{1-x})Pt^{4+}_2O_9$ phase with $x = 0.043(6)$ is described with a metrically orthorhombic unit cell $a_{orth} = 17.460(4)$ Å, $b_{orth} = 10.085(2)$ Å and $c_{orth} = 8.554(3)$ Å, and a monoclinic space group $C2$. The apparent hexagonal symmetry is caused by a merihedral twinning of the C-centered orthorhombic unit cell rotated around a pseudohexagonal axis parallel to the c axis. The weak correlation betwen neighboring –O–O–P– chains is due to the different distributions of three platinum atoms with respect to four barium planes along the c axis, and is described by translation domains. In each twins only D0, D1, and D2 domains exist, and trigonal prisms are always distributed in planes close to $(\bar{2}01)$ ones (Fig. 11). The main difference between P0–P1–P2 and P10–P11–P12 twins corresponds to a change in this prism distribution (for instance, the P10 individual has a prism distribution along (201) planes relative to a P0 reference). This could explain the two values for twin ratios: P0 ≈ P1 ≈ P2 ≈ 0.23 and P10 ≈ P11 ≈ P12 ≈ 0.10.

The sample order involves a prism distribution (along $(\bar{2}01)$) in large twins with only D0–D1–D2 translation domains (since D10–D11–D12 domains correspond to a presence of some local prism distribution along (201)). A local order exists for the Pt^{2+} cations inside each trigonal prism: this order requires low energy, and domains for Pt^{2+} distribution are too small to be described only by a twinning model. The difference of Pt^{2+} occupancies in each twin set (P0–P1–P2 or P10–P11–P12) is very small and is related to the small size of domains of the intraprism Pt^{2+} order. So, besides a low-symmetry space group and twinning, additional Pt^{2+} sites (Pt11, Pt33, Pt333) are needed in each domain for a complete description of the structure. This latter intraprism order exists only when Pt^{2+} cations are present in the structure ($x \neq 1.0$); however, when $x = 1.0$, a higher symmetry, without any twinning process, could be used but translation domains would probably exist.

TABLE 7
Interatomic Distances (in Å) of the Compound $Ba_4(Ba_x^{2+}Pt_{1-x}^{2+})Pt_2^{4+}O_9$, $x = 0.043(6)$

Pt2 +		Pt4 +		Pt2 +		Pt4 +		Pt4 +	
Pt1 O4	2.51(07)	Pt2 O4	1.89(07)	Pt33 O1	3.14(07)	Pt4 O5	2.00(13)	Pt5 O1	2.13(07)
	×2	Pt2 O6	2.08(09)	Pt33 O2	2.22(08)	Pt4 O8	2.07(07)	Pt5 O2	1.84(08)
Pt1 O6	2.37(08)	Pt2 O7	2.02(12)	Pt33 O3	1.96(11)	Pt4 O9	1.79(08)	Pt5 O3	2.09(11)
	×2	Pt2 O10	2.10(12)	Pt33 O11	2.86(11)	Pt4 O11	2.09(11)	Pt5 O5	2.15(12)
Pt1 O7	2.10(11)	Pt2 O10	2.17(12)	Pt33 O12	2.27(09)	Pt4 O12	1.94(09)	Pt5 O8	2.09(07)
	×2	Pt2 O14	2.07(13)	Pt33 O13	1.83(05)	Pt4 O13	1.95(05)	Pt5 O9	2.03(08)
Pt1 Pt2	2.947(08)	Pt2 Pt1	2.947(08)	Pt33 Pt4	3.119(08)	Pt4 Pt5	2.742(06)	Pt5 Pt33	2.894(08)
	×2	Pt2 Pt2	2.826(24)	Pt33 Pt5	2.894(08)			Pt5 Pt4	2.742(06)
Pt1 Ba2	3.398(17)	Pt2 Ba3	3.221(17)	Pt33 Ba1	3.235(12)	Pt4 Ba3	3.694(14)	Pt5 Ba1	3.382(12)
	×2	Pt2 Ba4	3.384(23)	Pt33 Ba3	3.370(19)	Pt4 Ba4	3.518(15)	Pt5 Ba2	3.299(22)
Pt1 Ba4	3.586(17)	Pt2 Ba5	3.428(19)	Pt33 Ba4	3.118(17)	Pt4 Ba5	3.518(18)	Pt5 Ba2	3.434(18)
	×2	Pt2 Ba6	3.690(22)	Pt33 Ba6	3.530(11)	Pt4 Ba6	3.330(12)	Pt5 Ba3	3.526(14)
		Pt2 Ba7	3.786(16)	Pt33 Ba6	3.530(11)	Pt4 Ba7	3.352(17)	Pt5 Ba4	3.559(15)
		Pt2 Ba7	3.526(16)			Pt4 Ba7	3.591(14)	Pt5 Ba5	3.502(17)

Ba1 O2	2.73(09)	Ba2 O1	2.75(07)	Ba3 O1	2.61(07)	Ba4 O2	2.98(08)	Ba5 O1	2.71(07)	Ba6 O4	3.39(07)	Ba7 O5	2.70(12)
	×2	Ba2 O1	2.86(08)	Ba3 O3	2.61(12)	Ba4 O2	2.81(08)	Ba5 O3	3.20(10)		×2	Ba7 O6	3.17(08)
Ba1 O3	2.92(10)	Ba2 O2	2.99(09)	Ba3 O4	2.63(07)	Ba4 O5	2.93(12)	Ba5 O4	3.10(07)	Ba6 O9	2.73(08)	Ba7 O7	3.08(11)
	×2	Ba2 O3	2.76(10)	Ba2 O5	2.90(12)	Ba4 O6	3.01(10)	Ba5 O6	2.86(10)		×2	Ba7 O8	2.74(07)
Ba1 O4	2.65(07)	Ba2 O5	2.84(11)	Ba3 O7	2.73(14)	Ba4 O7	2.93(14)	Ba5 O8	2.53(07)	Ba6 O10	3.04(13)	Ba7 O10	2.90(13)
	×2	Ba2 O6	2.61(09)	Ba3 O8	3.05(07)	Ba4 O9	2.98(09)	Ba5 O9	2.68(09)		×2	Ba7 O11	2.87(12)
Ba1 O9	3.08(08)	Ba2 O7	2.61(12)	Ba3 O10	2.74(12)	Ba4 O12	3.14(09)	Ba5 O10	2.69(13)	Ba6 O12	3.07(08)	Ba7 O11	3.15(12)
	×2	Ba2 O8	2.91(07)	Ba3 O11	3.34(10)	Ba4 O12	2.37(09)	Ba5 O11	2.49(11)		×2	Ba7 O12	2.65(08)
				Ba3 O13	2.80(05)	Ba4 O14	2.71(12)			Ba6 O13	2.87(05)	Ba7 O13	3.36(05)
											×2	Ba7 O14	2.86(02)

5. DIFFRACTION ANOMALOUS FINE STRUCTURE ANALYSIS

5.1. Principles

The real $f'(E)$ and imaginary $f''(E)$ anomalous components of the total atomic scattering factor are related to the absorption and contain value information on the electronic structure of atoms. Consequently, diffraction experiments, performed at several hundreds of energies over the absorption edge of a specific atom in the sample, present so-called diffraction anomalous fine structure (DAFS) oscillations and allow a site-selective chemical and local structural analysis for each independent "anomalous scatterer" present in the structure. As the DAFS technique combines the chemical and short-range structural sensitivity of absorption spectroscopy and the long-range structural selectivity of diffraction, it can provide site-selective spectroscopy information (21–25). This analysis includes an accurate anomalous scattering study and gives precise information on the occupancy and position of the absorbing atom in the sample.

The principles of DAFS were established a long time ago (26, 27) and were nicely developed in the 1990s by Stragier *et al.* (28) and Pickering *et al.* (22) on academic samples. To achieve a better accuracy on platinum occupancy on trigonal prismatic sites (without correlation with the twin/domain model used for the structural refinement), we performed anomalous scattering and DAFS analyses in the vicinity of the Pt L_{III} absorption edge on the same small twinned crystal of $Ba_4(Ba_xPt_{1-x}^{2+})Pt_2^{4+}O_9$. These experiments also give additional information on the platinum valence state on the octahedral site.

5.2. Intensity Simulations versus Energy

As in our sample no reflection has a systematic contribution of Pt atoms in only one site (the trigonal prismatic one or the octahedral one), we have to calculate their contributions to the diffracted intensities. Calculations were performed using, as initial values, $f'(E)$ and $f''(E)$ curves of free atoms given by Sasaki (29) and refined atomic positions (Table 6). We chose some reflections having nearly zero Pt contribution (1.5% for (352) and $(\bar{3}52)$), since their intensity variations are affected mainly by bulk absorption. To extract DAFS information from both sites, we selected several

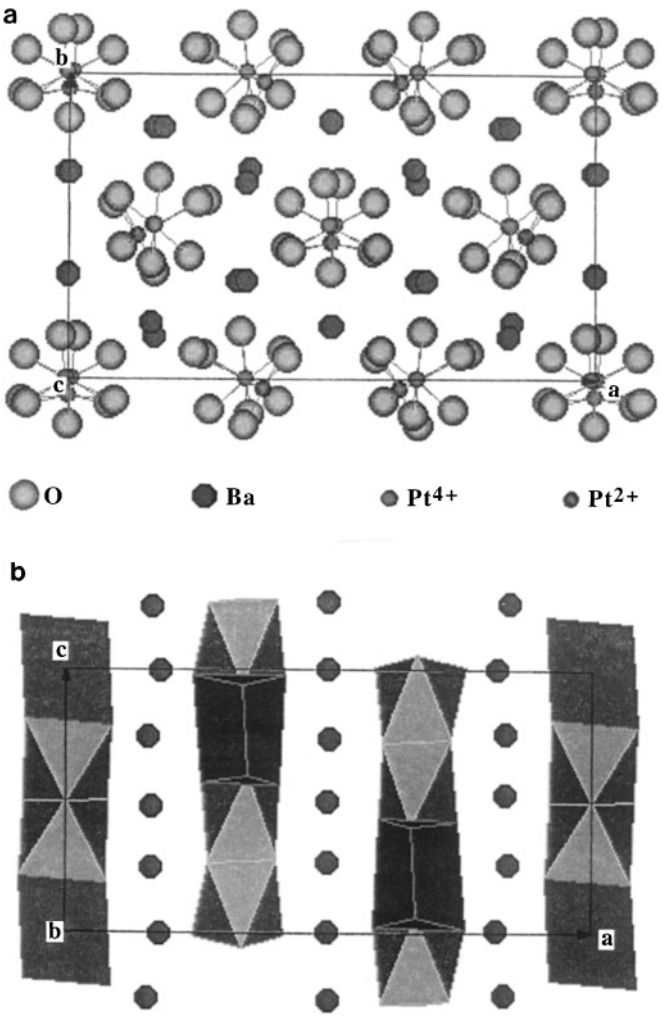

FIG. 12. Structure of the compound $Ba_4(Ba^{2+}_xPt^{2+}_{1-x})Pt^{4+}_2O_9$, $x = 0.043(6)$. (a) Projection in the (a, b) plane of atomic positions in the D0 domain. (b) Distribution of the –O–O–P– chains along the c axis in the same domain.

reflections for their higher contribution of Pt atoms in the octahedral sites (as examples (263) and ($\bar{2}63$)). However, due to the presence of twinning domains in the structure, it was not possible to select reflections highly sensitive to the Pt atoms in the trigonal prismatic sites.

For these last intensity simulations, we used the chemical sensitive $f''_{Pt}(E)$ anomalous factors, extracted from the absorption spectra of Pt^{4+} and Pt^{2+} cations measured on reference samples, and $f'_{Pt}(E)$ calculated by Kramers–Kronig relation:

$$f''_{Pt}(E) = \frac{mcE}{4he^2}\,\sigma_{Pt}(E),$$

$$f'_{Pt}(E) = \frac{2}{\pi}\int_0^{\infty} \frac{E' f''_{Pt}(E')}{E^2 - E'^2}\,dE',$$

where σ_{Pt} is the atomic cross section of platinum atom, m is the electron mass, c is the velocity of light, h the Planck constant, and e is the electron charge.

As the crystal is twinned, the intensity contribution of each individual to a given (hkl) Bragg peak must be calculated. In Fig. 13 we present an example of these intensity simulations with $f'f''_{Pt^{4+}}(E)$ and $f'f''_{Pt^{2+}}(E)$ for two reflections: (443) sensitive to trigonal prismatic site and (263) sensitive to octahedral site. We compare them to the simulation obtained with the average $f'_{Pt}(E)$ and $f''_{Pt}(E)$ factors extracted from the bulk absorption spectrum of the crystal. The absence of difference for the (263) reflection sensitive to the Pt^{4+} site is normal, since the bulk absorption spectrum is close to the Pt^{4+} reference one. However, for the (443) reflection (sensitive to the Pt^{2+} site), there is a weak difference for only one twinned domain (P2), and this reflection overlaps much stronger reflections coming from domains P12, P10, and P11. This means that we could extract DAFS information only for the octahedral site. Finally, the following 24 reflections were selected for the DAFS data collection:

(135), (463), (246), (243), (443), (553), (263), (193), (593), (334), (352), (354),

and

($\bar{1}35$), ($\bar{4}63$), ($\bar{2}46$), ($\bar{2}43$), ($\bar{4}43$), ($\bar{5}53$), ($\bar{2}63$), ($\bar{1}93$), ($\bar{5}93$), ($\bar{3}34$),($\bar{3}52$), ($\bar{3}54$).

5.3. Data Collection

Diffraction intensities were measured as a function of the X-ray energy by scanning through the Pt L_{III} absorption edge. The experiment was performed on the diffraction station WDIF4C of the DCI-LURE synchrotron radiation facility. A Si(111) double-crystal monochromator and a scintillation detector were used. Reflections ($\bar{1}35$) and (135), having a large Pt contribution from the trigonal prismatic sites, were too weak, so only diffracted intensities of the remaining 22 reflections were collected in the 11500–11700 eV energy range. A 2 eV step was chosen in the vicinity of the L_{III} edge and 4 eV step far from the edge. For energy calibration, a sample fluorescence spectrum was measured simultaneously with the single-crystal data collection. Because of the sample dimension which was smaller than the incident beam, and because of inhomogeneities of the beam, this crystal fluorescence spectrum was very important as an additional monitor of the incident beam.

5.4. Intensity Refinements

The collected intensities are the sum of contributions from different domains that were corrected for the absorption and Lorentz–polarisation factors, and they correspond to

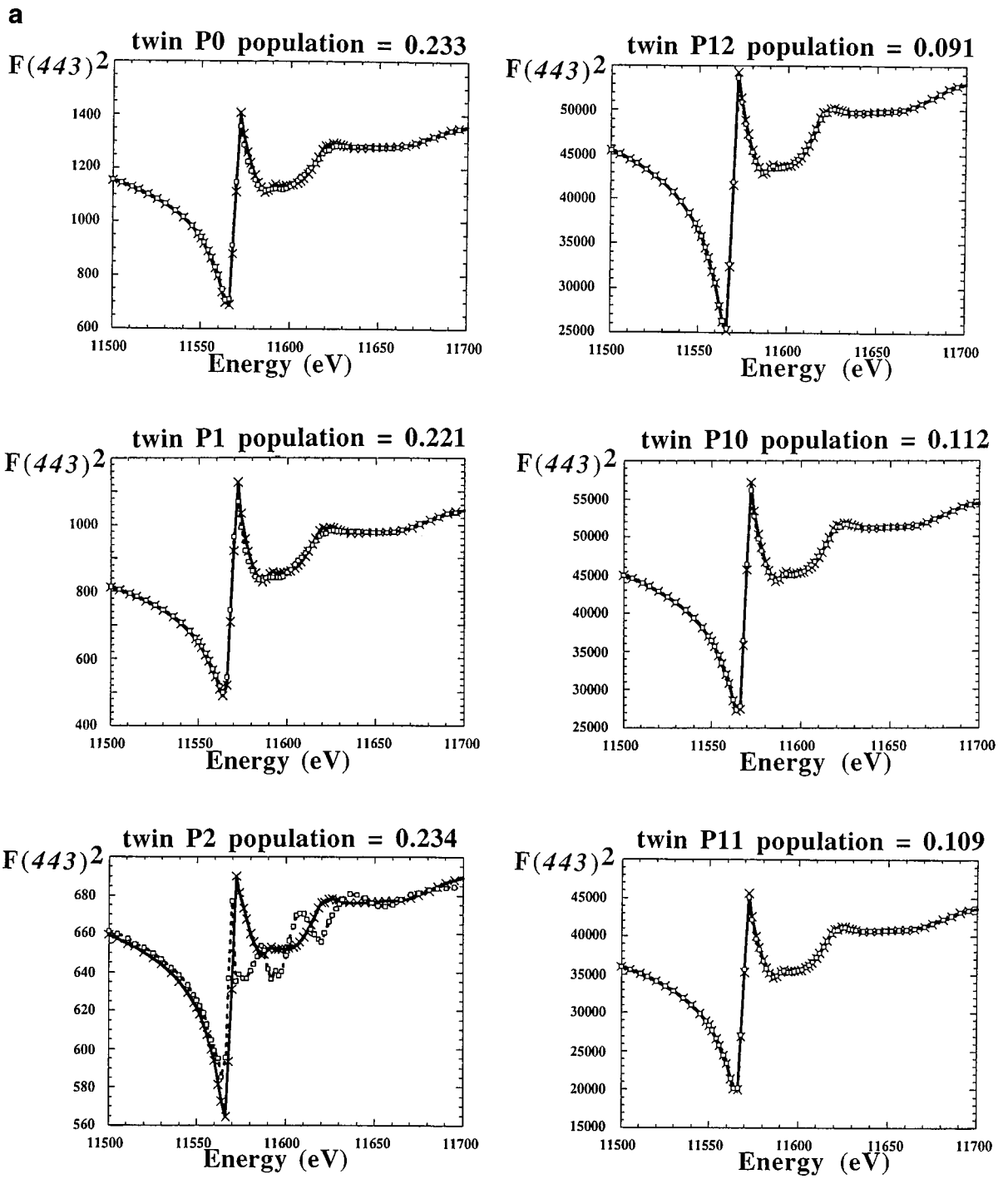

FIG. 13. Structure factor simulations for all different twinned domains, using $f'f''_{Pt^{4+}}(E)$ and $f'f''_{Pt^{2+}}(E)$ factors (dotted line and open square), and using the average $f'_{Pt}(E)$ and $f''_{Pt}(E)$ factors extracted from the bulk absorption spectrum of the crystal (full line and crosses). (a) (443) reflection with some Pt^{2+} contribution. (b) (263) reflections with a preponderant Pt^{4+} contribution.

$$I(hkl) = C_0 LP\,\mathrm{Abs}\,\frac{D}{E^3}\left(|F_T|^2 + \frac{(f'^2_{Pt} + f''^2_{Pt})}{f^{\circ 2}_{Pt}}|F_{Pt}|^2 + 2\frac{f'_{Pt}}{f^{\circ}_{Pt}}|F_T||F_{Pt}|\cos(\Delta\Phi) + 2\frac{f''_{Pt}}{f^{\circ}_{Pt}}|F_T||F_{Pt}|\sin(\Delta\Phi)\right),$$

where C_0 is a scale factor, LP is the Lorentz–polarization correction, Abs the transmission coefficient due to absorption correction, D the detector efficiency and the air path absorption, F_T the module of the "constant" structure factor of all atoms (Thomson and anomalous scattering terms of

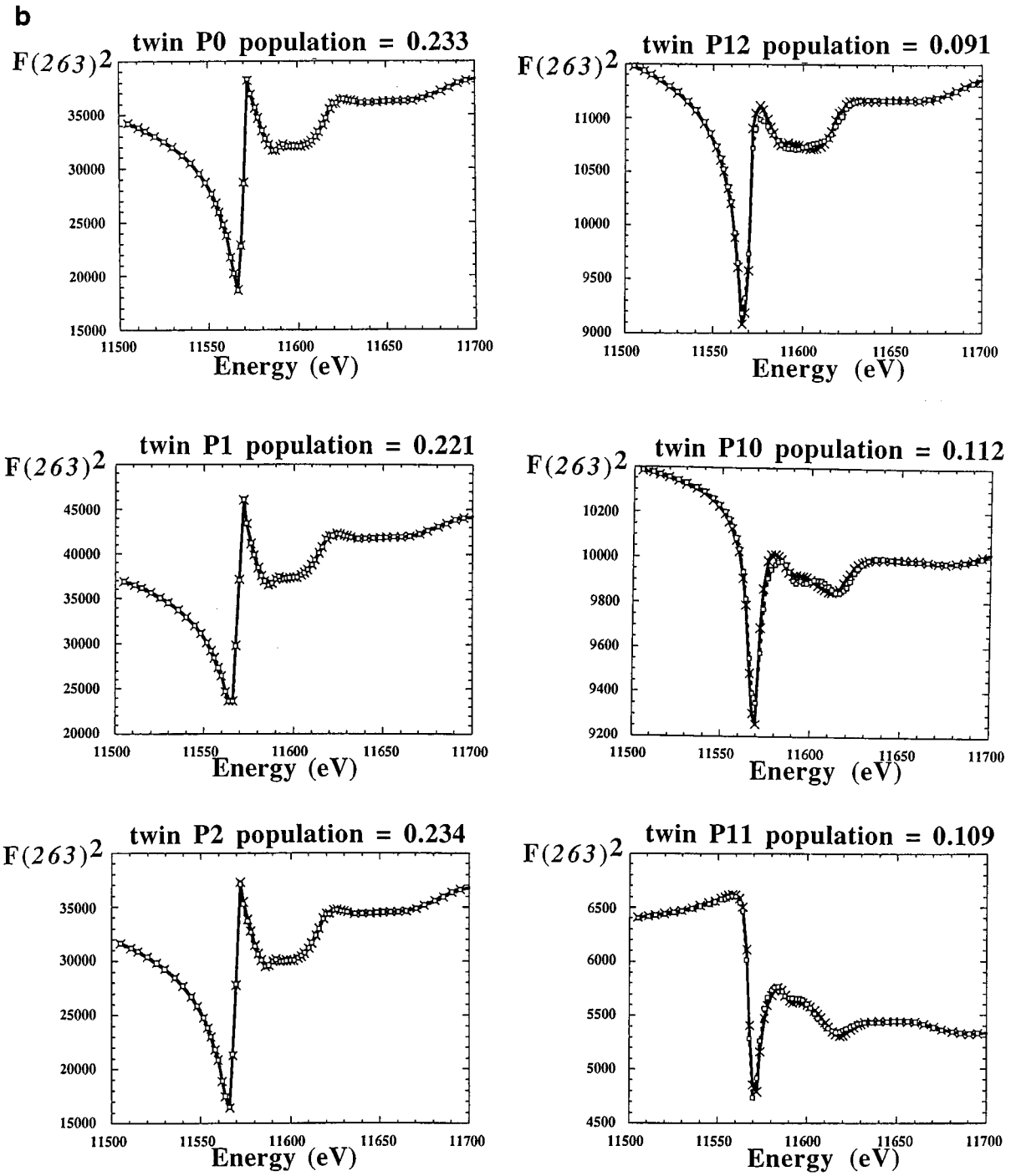

"non anomalous atoms" and Thomson scattering terms of platinum), F_{Pt} the module of the "constant" structure factor of platinum (Thomson scattering terms), $\Delta\Phi = \Phi_T - \Phi_{Pt}$ the phase difference between phase of structure factor of all atoms (Φ_T) and those of platinum atoms (Φ_{Pt}), f°_{Pt}, f'_{Pt}, and f''_{Pt} the Thomson, real, and imaginary scattering factors of platinum, respectively.

For the data analysis and refinement, we proceeded as follows.

(1) A precise absorption correction was applied by using transmission absorption measurements.

(2) A complete structure factor calculation was developed with a complex scaling correction to obtain the best fitting of intensity curves far from the edge.

(3) A simultaneous refinement of several reflections at all energies was performed by a least-squares procedure with f'_{Pt} as variable.

(4) f''_{Pt} values were determined by Kramers–Kronig relations from the refined f'_{Pt} terms.

As the Pt proportion is important in our sample, the absorption is large at the Pt edge and the first observable effect on diffraction intensities is the jump and oscillations corresponding to bulk absorption. Thus a precise absorption correction must be carried out (an increase of sample dimension of 2 μm gives rise to intensity variations ranging from 7 to 15% depending on energy and reflection). We developed an empirical absorption correction which takes into account the crystal shape (truncated hexagonal polyhedron, $150 \times 130 \times 70$ μm) and refined a deviation of sample thickness Δt from the intensity variation before and after the edge (15). As the absorption jump is also sensitive to platinum content and consequently to the $(Ba_xPt^{2+}_{1-x})$ occupancy of the trigonal prism site of the $Ba_p(Ba_xPt^{2+}_{1-x})Pt^{4+}_{p-2}O_{3p-3}$ crystal (Fig. 14), intensity versus energy spectra were used to refine both this mixed occupancy and the thickness deviation. Using the structure model, the values x and $\Delta t(hkl)$ were refined for the 22 reflections in the energy regions before and ~ 60 eV after the absorption edge by the program MXD (20). The values $\Delta t(hkl)$ vary between ± 7 µm and $x = 0.08(2)$ with $R = 4.7\%$. Recall that the x value obtained from complete structure refinement with domains and monochromatic data is $x = 0.043(6)$. Although more peaks are used in the single-wavelength refinement, the high sensitivity of the anomalous scattering to mixed site occupancy makes the value $x = 0.08$ more reliable. Example of final intensity fits applying the absorption correction procedure are shown in Fig. 15 for the two reflections (443) and (263) where, due to the different domain contributions, no sensitivity to the Pt^{2+} site remains.

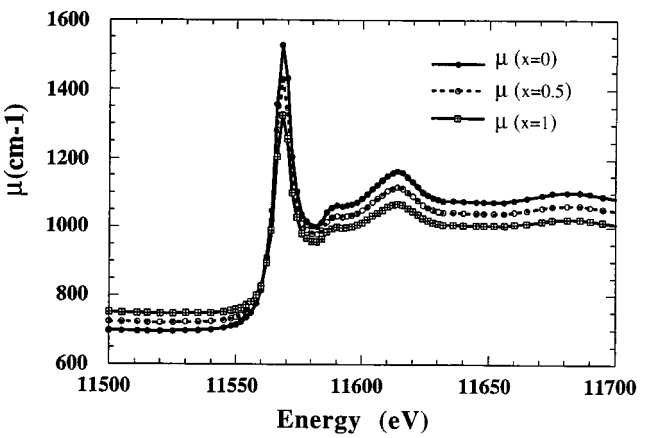

FIG. 14. Absorption coefficient of $Ba_4(Ba^{2+}_xPt^{2+}_{1-x})Pt^{4+}_2O_9$ for different Ba content (x).

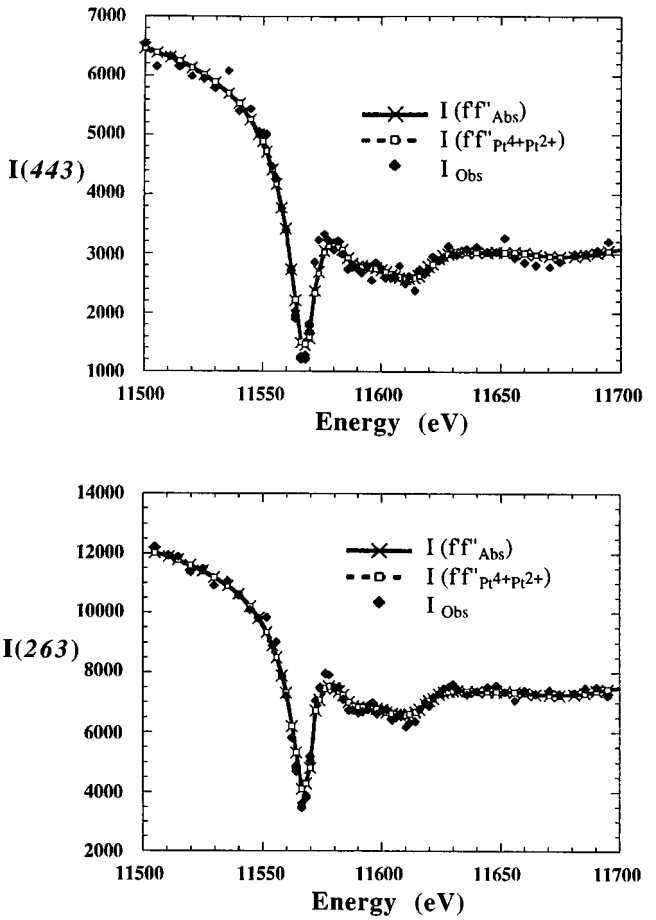

FIG. 15. Observed and calculated intensity variation versus energy of (a) (443) reflection with some Pt^{2+} contribution. (b) (263) reflections with a preponderant Pt^{4+} contribution.

The refined f''_{Pt} anomalous scattering factor for the octahedral site is reported in Fig. 16. We can clearly see on the f''_{Pt} curve the intense "white" line at 11564 eV characteristic of the Pt^{4+} chemical state. With respect to the f''_{Abs} curves, obtained directly from transmission absorption experiment performed on the powdered sample, the f''_{Pt} factor for the octahedral site presents a stronger white line. It indicates the probable contribution of a mixture of Pt^{4+} and Pt^{2+} in the bulk absorption signal f''_{Abs}.

6. DISCUSSION AND CONCLUDING REMARKS

Three approaches can be envisaged to analyze partially ordered systems.

(a) Refine the structure with an average structural model using the highest possible symmetry and partial occupancy of atoms (3, 16, and Section 4.5 herein],

(b) Refine the structure using a continuous mathematical representation of a modulated structure which is able to explain a continuous deformation of a basic unit cell. In this

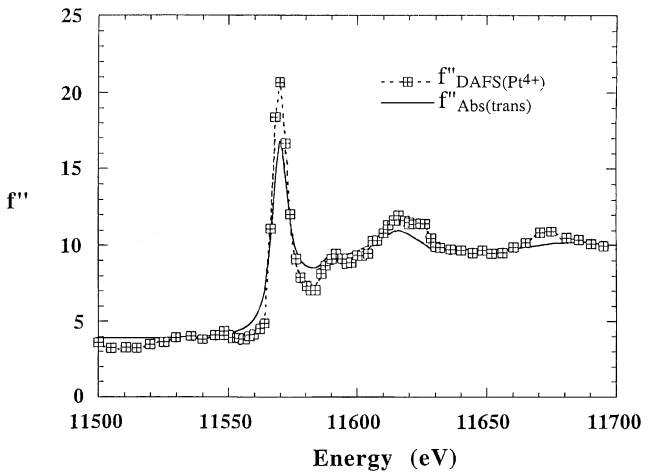

FIG. 16. f'' anomalous curves extracted from DAFS (dotted line) and XAFS (solid line) experiments.

case, as in the case of $[Ba]_x[(Pt, Cu)O_3]$ (13), this representation describes the coexistence of two distinct structural entities: *barium planes* and *platinum chains.*

(c) Find the relations and mechanisms of structural faults, define an ordered structural unit, and refine the structure taking into account the influence of all faults on this ordered entity [Section, 4.6 herein].

Choice (a) is mathematically the simplest, but it can induce errors in the interpretation. In our refinement, this choice corresponds to the structural model described with the hexagonal unit cell and the space group *P*321. Our results clearly show that this model does not completely take into account diffracted intensities. In addition, the model cannot give an unambiguous answer about the local environment of Pt^{2+} cations. This "average" model represents relatively well the structure and the chemical reality of the sample with the limiting condition that the twins, producing the pseudohexagonal symmetry, have comparable sizes. In fact, this description is correct if domains generated by faults are very small. However the interatomic distances obtained in such refinements are only average distances.

With choice (b), the structure is nicely described with a regular modulated wave. It is found to be very efficient in cases where few satellite spots are generated around basic structure reflections (charge density wave). In our case, as for $[Ba]_x[(Pt, Cu)O_3]$, the structure is very close to a composite one, which gives rise to two reciprocal lattices in the diffraction patterns. These two lattices can be interpreted and described by a modulation wave. However, the description by position waves, which gives the evolution of different sites along the modulation direction, is global and cannot easily describe the local structural entity and discontinuities generated by faults.

With respect to the results obtained from electron diffraction and X-ray precession, indicating the existence of faults, domains, and twins, the third possibility (c) seems to us more appropriate to fully describe the structure of $Ba_4(Ba_xPt^{2+}_{1-x})Pt^{4+}_2O_9$. Such a description allows an estimation of the domain ratio and, consequently, a determination of fault types and proportions (Table 4, Fig. 11). It further allows the visualization of the local structure inside each domain (Fig. 12).

From the refined ratio of these domains, we can estimate the most energetically favorable faults (intra- or interchains trigonal prism distribution, Pt^{2+} position on prism faces). The intrachain –O–O–P– distribution is nearly perfect. Its corresponding oxygen deficiency is given directly by the modulus of the $\mathbf{q}^*_c$ modulation vector, via the equation $\mathbf{q}^*_c = 2/p$ and $p \sim 4$ in the formula $Ba_p(Ba_xPt^{2+}_{1-x})Pt^{4+}_{p-2}O_{3p-3}$. The misfit between the platinum chains and the Ba framework gives rise to an incommensurate intrachain distribution ($q^*_c = 0.507$). The interchain order is not perfect; it corresponds to a prism distribution along planes close to $(\bar{2}01)$ ones with some translation faults (D0, D1, and D2) and gives rise to large ordered twinned domains (P0, P12, P1, P10, P2, P11). Inside the trigonal prisms of these domains, faults in the Pt^{2+} positions on rectangular faces are energetically favorable, and the sizes of perfect ordered units such as those represented in Fig. 12 are quite small.

The $Ba_p(Ba_xPt^{2+}_{1-x})Pt^{4+}_{p-2}O_{3p-3}$ series exists for $p = 3, 4, 5, \ldots, \infty$ where some of them correspond to ordered compounds (Table 1). As it was found for the Magneli phases M_pO_{2p-1} (M = Ti, V, $p = 2, 3, 4, \ldots, \infty$), some intrachain disorder could occur for large p and for compositions close to $BaPtO_3$, where the –O–O–O–O–P– periodicity are less defined (as is the case for shear plane distribution in $TiO_{2-\delta}$ compounds). For small p, ordered intrachain compounds are formed, and their symmetry is directly related to the $(Ba_xPt^{2+}_{1-x})$ occupancy of a trigonal prism. In these sites, Ba atoms are at the center of trigonal prisms and a high Ba occupancy favors the Pt^{2+} disorder on trigonal prism faces. In such a case (x close to 1), the structural description in the hexagonal space group could be more appropriate (taking into account the translation domains). Thus, the hexagonal symmetry corresponds to a Ba^{2+} full occupancy, and the pseudohexagonal twinning to a Pt^{2+} occupancy.

The interchain disorder points out the weak chemical bonding between the barium framework and the $–PtO_3–$ chains, and the composite nature of this series. Its one-dimensional character is important for the anisotropic physical properties, and we could expect that properties such those found in $Sr_3Cu(Ir_xPt_{1-x})O_6$ (14) could also exist in the $Ba_p(Ba_xPt^{2+}_{1-x})Pt^{4+}_{p-2}O_{3p-3}$ series, if we replace $(Ba_xPt^{2+}_{1-x})$ sites by copper cations. In this last case, we could also vary the intrachain interaction between Cu atoms by increasing the distances between trigonal prismatic sites (variation of p parameter). Structural properties and defects in this series can be also extrapolated to similar

existing compounds by substitution of barium by strontium atoms and platinum by iridium or ruthenium atoms.

ACKNOWLEDGMENTS

We thank Prof. B. L. Chamberland for providing the samples, Dr. E. El Kaïm and Prof. J. P. Lauriat, from the LURE facility, for their kind help with the synchrotron data collection, and Dr. P. Wolfers for his assistance and helpful discussions during the structural refinements.

REFERENCES

1. K. B. Schwartz and C. T. Prewitt, *J. Phys. Chem. Solids* **45,** 1 (1984).
2. S. J. Schneider and C. L. McDaniel, *J. Am. Ceram. Soc.* **52,** 518 (1969).
3. P. S. Haradem, B. L. Chamberland, L. Katz, and A. Gleizes, *J. Solid State Chem.* **21,** 217 (1977).
4. B. L. Chamberland, The Study of Ternary Ba–Pt–O. Research Proposal.
5. P. K. Gallagher, D. W. Johnson, E. M. Vogel, G. K. Wertheium, and F. J. Schnettler, *J. Solid State Chem.* **21,** 277 (1977).
6. A. P. Wilkinson and A. K. Cheetham, *Acta Crystallogr. Sect. C* **45,** 519 (1959).
7. J. J. Randall and L. Katz, *Acta Crystallogr.* **12,** 1672 (1989).
8. L. Ben-Dor, J. T. Suss, and S. Cohen, *J. Cryst. Growth* **64,** 395 (1983).
9. A. P. Wilkinson, A. K. Cheetham, W. Kunnmann, and Å. Kvick, *Eur. J. Solid State Inorg. Chem.* **28,** 453 (1991).
10. J. L. Hodeau, H. Y. Tu, P. Bordet, T. Fournier, P. Strobel, and M. Marezio, *Acta Crystallogr. Sect. B* **48,** 1 (1992).
11. C. L. Mc Daniel, *J. Am. Ceram. Soc.* **55,** 426 (1972).
12. Z. Czaya, *Z. Anorg. Allg. Chem.* **375,** 61 (1970).
13. K. Ukei, A. Yamamoto, Y. Watanabe, T. Shishido, and T. Fukuda, *Acta Crystallogr. Sect. B* **49,** 67 (1993).
14. T. N. Nguyen, P. A. Lee, and H.-C. zur Loye, *Science* **271,** 489 (1996).
15. J. Vacínová, J. L. Hodeau, P. Wolfers, E. El Kaim, J. P. Lauriat, B. Bouchet-Fabre, and B. L. Chamberland, *Nucl. Instr. Meth. Phys. Res. B* **97,** 102 (1995).
16. F. Grasset, F. Well, and J. Darriet, *J. Solid State Chem.* **140,** 194 (1998).
17. C. Dussarat, J. Fompeyrine, and J. Darriet, *Eur. J. Solid State Inorg. Chem.* **32,** 3 (1995).
18. D. T. Cromer, and J. T. Waber, *Acta Crystallogr.* **15,** 104 (1965).
19. D. T. Cromer, and D. Liberman, *J. Chem. Phys.* **53,** 1981 (1970).
20. P. Wolfers, *J. Appl. Crystallogr.* **23,** 554 (1990).
21. L. B. Sorensen, J. O. Cross, M. Newville, B. Ravel, J. J. Rehr, H. Stragier, C. E. Boulin, and J. C. Woicik, *in* "Resonant anomalous X-ray scattering" (G. Materlink, C. J. Sparks, and K. Fischer, eds.), p. 389. Elsevier Science B. V., Amsterdam, 1994.
22. I. J. Pickering, M. Sansone, J. March, and G. N. George, *J. Am. Chem. Soc.* **115,** 6302 (1993).
23. J. L. Hodeau, J. Vacínová, Y. Garreau, A. Fontaine, Hagelstein, E. El Kaïm, J. P. Lauriat, A. Prat, and P. Wolfers, *Rev. Sci. Instrum.* **66,** 1499 (1995).
24. J. Vacínová, J. L. Hodeau, P. Wolfers, J. P. Lauriat, and E. El Kaïm, *J. Synchrotron Rad.* **2,** 236 (1995).
25. H. Renevier, J. L. Hodeau, P. Wolfers, S. Andrieu, J. Weigelt, and R. Frahm, *Phys. Rev. Lett.* **78,** 2775 (1997).
26. Y. Cauchois and C. Bonnelle, *C. R. Acad. Sci.* **242,** 1596 (1956).
27. I. Arcon, A. Kodre, D. Glavic, and M. Hribar, *J. Phys. C* **9,** 1105 (1987).
28. H. Stragier, J. O. Cross, J. J. Rehr, L. B. Sorensen, C. E. Boulin, and J. C. Woicik, *Phys. Rev. Lett.* **21**(69)**,** 3064 (1992).
29. S. Sasaki, "Anomalous Scattering Factors for Synchrotron Radiation Users." National Laboratory for High Energy Physics, Report, Japan, 1984.